Euclid: Globular cluster timing problem in local Universe dwarf galaxies: evidences for dynamical friction counteracting mechanisms★

P. Boldrini ★★[1], T. Saifollahi[2], A. Claeyssens[3], A. Lançon[2], and al.

(*Affiliations can be found after the references*)

July 20, 2026

ABSTRACT

Key words. Galaxies: clusters: individual: Perseus – Galaxies: star clusters: general

1. Introduction

The Fornax dwarf spheroidal galaxy is an exceptional laboratory for investigating dark matter (DM) dynamics. Dwarf galaxies are among the most DM-dominated systems in the Universe, and their internal dynamics are largely controlled by their host DM halos (Battaglia et al. 2013; Walker 2013). As one of the most massive satellites of the MW, Fornax has a stellar mass of approximately $2{-}4{\times}10^7$, $M_\odot$ (Mateo 1998; de Boer & Fraser 2016; Borukhovetskaya et al. 2022). It is also distinguished by its rich globular cluster (GC) system, hosting five confirmed GCs and possibly a sixth candidate, an unusually large population for a galaxy of this mass (Mackey & Gilmore 2003; de Boer & Fraser 2016; Wang et al. 2019; Forbes et al. 2018). Cosmological hydrodynamical simulations from the E-MOSAICS project further emphasize the rarity of this system, predicting that only 3% of Fornax analogues contain five or more GCs, while 35% host no GCs at all (Shao et al. 2021).

The presence of these old GCs (ages between 10 and 12 Gyr) at galactocentric distances of the order of a kiloparsec gives rise to the long-standing "Fornax timing problem". First formulated by Oh et al. (2000), the problem arises from the apparent inconsistency between the present-day locations of the GCs and their expected orbital decay due to dynamical friction. If the GCs formed near their current positions, they should have spiralled into the centre of Fornax within only a few Gyr, significantly shorter than their inferred ages, potentially leading to the formation of a nuclear star cluster (NSC). However, no such massive NSC is observed. Dynamical friction occurs when a massive object moves through a background of lighter particles, such as DM particles and field stars, generating a gravitational wake that trails behind it (Chandrasekhar 1943). This overdensity exerts a drag force on the object, causing it to lose orbital energy and angular momentum and gradually sink toward the centre of its host galaxy. In the cuspy Navarro-Frenk-White (NFW) DM halos predicted by the CDM paradigm (Navarro et al. 1996, 1997a), the corresponding orbital decay timescales are typically estimated to be between 1 and 5 Gyr, much shorter than the ages of the Fornax GCs. Under these conditions, the clusters are expected to merge in the central regions and form a massive NSC (Tremaine 1976; Tremaine et al. 1975; Oh et al. 2000). Historically, Fornax has been considered a non-nucleated dwarf galaxy, strengthening the tension between theoretical expectations and observations. Indeed, Cole et al. (2012a) estimated that, in a cuspy DM halo, the probability that none of the GCs reaches the centre within 2 Gyr is less than 2%. However the recently rediscovered sixth GC (GC6), located at a projected distance of only ~ 0.27 kpc from the centre of Fornax, could represent the long-sought NSC. Although this low-mass cluster ($\sim 10^4$ $M_\odot$) exhibits signs of tidal disruption consistent with ongoing orbital decay, its existence does not fully resolve the timing problem. The most massive clusters, such as GC3 and GC4, are still observed at substantially larger radii despite being expected to experience stronger dynamical friction and therefore to sink more rapidly than GC6. This apparent discrepancy between the observed distribution of the Fornax GCs and the predictions of dynamical friction has been recognized for more than 25 years and has motivated a large body of theoretical work. Proposed solutions generally invoke either modifications to the internal structure of the DM halo or specific orbital histories of the GCs, with the common goal of reducing or counteracting the efficiency of dynamical friction.

One of the most extensively explored solutions to the Fornax timing problem involves the internal structure of the DM halo itself (Goerdt et al. 2006a; Read et al. 2006a; Cole et al. 2012a; Sánchez-Salcedo et al. 2006a; Inoue 2009; Kaur & Sridhar 2018; Meadows et al. 2020; Boldrini et al. 2019). This directly connects the timing problem to the cusp-core problem in ΛCDM paradigm (Bullock & Boylan-Kolchin 2017; Boldrini 2021). In the standard paradigm, DM halos are expected to develop cuspy density profiles characterized by a steep central density $\propto r^{-1}$). In such halos, dynamical friction remains highly efficient, making the orbital decay of massive GCs toward the galactic centre almost unavoidable (Tremaine 1976; Hernandez & Gilmore 1998). In contrast, numerous observational studies have suggested that some galaxies may instead host cored DM halos, whose central density approaches a constant value rather than diverging toward the centre (Flores & Primack 1994; Moore 1994; McGaugh et al. 2001a; Oh et al. 2011, 2015a; Oman et al. 2015; Santos-Santos et al. 2020a; Adams et al. 2014; Brook 2015). Evidence from stellar kinematics in dwarf galaxies has also been interpreted as favouring cored DM distributions (Strigari et al.

★ This paper is published on behalf of the Euclid Consortium

★★ e-mail: pierre.boldrini@obspm.fr

2006; Walker & Peñarrubia 2011; Burkert 2015; Amorisco et al. 2013). In such halos, dynamical friction is significantly weakened and GCs are expected to stall at a characteristic radius, typically located at roughly one-third of the core radius (Goerdt et al. 2006a; Read et al. 2006a; Petts et al. 2015; Meadows et al. 2020). As a result, GCs can survive for a Hubble time without reaching the galactic centre. Within the CDM framework, cored density profiles may arise through the baryonic feedback processes during galaxy formation (Pontzen & Governato 2012; Di Cintio et al. 2014; Tollet et al. 2016). However, the efficiency and ubiquity of this mechanism remain actively debated. In DM-only simulations, such cores do not emerge naturally, making their existence dependent on complex baryonic processes. By contrast, central cores arise naturally in several alternative DM scenarios, including self-interacting DM (Kaplinghat et al. 2016) and fuzzy DM (Schive et al. 2014). Some cored halo models even predict the onset of dynamical buoyancy, whereby GCs gain orbital energy through interactions with fast-moving background particles and migrate outward from the central regions. This mechanism can further suppress orbital decay and extend cluster survival well beyond a Hubble time (Cole et al. 2012a; Dattathri et al. 2025).

However, the core solution is challenged both by the absence of a common stalling radius for the five Fornax GCs and by the uncertain origin of DM cores within the CDM framework. Consequently, additional dynamical mechanisms have been proposed to explain the long-term survival of the GCs. One possibility is to increase the orbital decay timescales by assuming that the GCs formed at larger galactocentric distances than those observed today, rather than near their present-day locations (Cowsik et al. 2009; Cole et al. 2012a; Arca-Sedda & Capuzzo-Dolcetta 2016; Boldrini et al. 2019; Meadows et al. 2020; Sánchez-Salcedo & Lora 2022). If the GCs originated sufficiently far from the galactic centre, the time required for dynamical friction to drive them inward can exceed the age of the Universe, even within a cuspy halo. However, Sánchez-Salcedo & Lora (2022) showed that relatively small variations (±20%) in the assumed initial radii can lead either to rapid infall toward the centre or to long-term survival within the galaxy. Moreover, given the measured ages of the GCs (10-12 Gyr), it remains unclear whether the gas density in the high-redshift progenitor of Fornax would have been sufficient to support GC formation at such large galactocentric distances, particularly given the more compact structure expected for dwarf galaxies at early times (Leung et al. 2020a).This scenario naturally raises the possibility that some of the Fornax GCs were accreted rather than formed in situ. In that case, GCs acquired through past merger events would have started experiencing dynamical friction within the Fornax potential only after their accretion, substantially reducing the time available for orbital decay. In support of this picture, Shao et al. (2021) found that the GC populations of Fornax analogues in the E-MOSAICS simulations are composed of nearly equal fractions of in situ (45%) and ex situ (55%) GCs. Furthermore, a major merger with a mass ratio of approximately 1:5 or 1:2 could have transferred angular momentum to the GC system, causing the orbits of pre-existing clusters to expand and further delaying their inward migration (Leung et al. 2020a). Such merger-driven processes are particularly attractive because they may alleviate the need for all GCs to share a common stalling radius. In addition, the unusually large total mass of the Fornax GC system relative to its metal-poor field-star population would be easier to reconcile if one or more of the GCs were accreted from external galaxies (Larsen et al. 2012). An alternative scenario was proposed by Boldrini et al. (2020a), who explored the possibility that the Fornax GCs formed within their own DM minihalos ($\sim 10^7$ $M_\odot$). Although these systems initially experience stronger dynamical friction because of their larger total masses, repeated passages through the central regions of Fornax dynamically heat the host DM halo and progressively transform its inner density profile from a cusp into a core. This cusp-to-core transition subsequently reduces the efficiency of dynamical friction, slowing further orbital decay. At the same time, the surrounding DM minihalos protect the stellar components of the clusters from the tidal forces exerted by the host galaxy, thereby enhancing their long-term survival (Boldrini et al. 2020a; Vitral & Boldrini 2022).

Additional solutions have focused on uncertainties in one property of Fornax and on the influence of its environment. In particular, the total DM halo mass of Fornax remains uncertain by nearly an order of magnitude, with estimates ranging from $\sim 10^9, M_\odot$ based on stellar kinematics (Goerdt et al. 2006a; Battaglia et al. 2006; Errani et al. 2018; Walker et al. 2009; Wolf et al. 2010; Read & Erkal 2019) to $\sim 10^{10}, M_\odot$ from abundance-matching models (Wang et al. 2015; Fattahi et al. 2018; Garrison-Kimmel et al. 2019; Munshi et al. 2021; Behroozi et al. 2010). If Fornax was originally substantially more massive before undergoing tidal stripping by the MW, the resulting lower central densities would reduce the efficiency of dynamical friction and increase the orbital decay timescales of its GCs. The role of the Galactic environment has also been examined. As a satellite of the MW, Fornax evolves within the Galactic potential and may experience tidal perturbations during pericentric passages along its orbit (Oh et al. 2011; Borukhovetskaya et al. 2022). Although Galactic tides can modify the orbital properties of GCs, for example by increasing their eccentricities, their impact on the final orbital decay timescale appears to be secondary compared to the influence of the internal DM distribution of the host galaxy (Borukhovetskaya et al. 2022). Tidal interactions may also reshape the DM halo itself and potentially reduce the central density of an initially cuspy profile. However, numerical studies suggest that tidal stripping primarily affects the outer regions of dwarf galaxies, while leaving the inner density profile largely intact (Peñarrubia et al. 2008; Genina et al. 2022). This is particularly relevant for Fornax, which currently resides at a large Galactocentric distance (∼ 149 kpc) and follows a relatively low-eccentricity orbit around the MW (Pietrzyński et al. 2009; Piatek et al. 2002; Dinescu et al. 2004; Battaglia et al. 2015; Lux et al. 2010; Gaia Collaboration et al. 2018a).

The Fornax timing problem remains a fundamental challenge for our understanding of dwarf galaxy dynamics and the nature of DM. In this context, the Euclid mission provides an unprecedented opportunity to revisit this long-standing issue on a much larger scale, using a sample of dwarf galaxies and associated GCs that is orders of magnitude larger than previously available. Until now, this problem has been investigated almost exclusively in the Fornax dwarf spheroidal galaxy, largely because it is the only satellite dwarf of the MW known to host such a rich GC system, while comparable datasets have remained unavailable for other dwarfs. The Euclid Early Release Observations (ERO, Cuillandre et al. 2025a) have fundamentally changed this situation. For the first time, they provide access to the same key observables that originally motivated the Fornax study, namely the projected galactocentric distances and masses of GCs hosted by dwarf galaxies.

In this paper, we revisit the Fornax timing problem in the local Universe using the Euclid ERO sample of more than 6,000 GCs hosted by over 800 dwarf galaxies in the Fornax and

Perseus galaxy clusters. Our goal is to determine whether the timing problem is a unique feature of the Fornax dwarf galaxy or a generic outcome of GC evolution in dwarf galaxies. To this end, we estimate GC orbital decay timescales using the classical dynamical friction framework and explore the impact of the main solutions proposed in the literature to mitigate dynamical friction. The paper is structured as follows: Section 2 outlines our methodology, including the Euclid globular cluster and dwarf galaxy samples, the adopted mass models, and the orbital integrations with dynamical friction. In Section 3, we present and discuss our results, focusing on the timing problem in local Universe dwarf galaxies and on the implications on the origin of globular clusters. Finally, Section 4 summarizes our main conclusions.

2. Methods

Our approach is based on combining the most recent observations of globular clusters in dwarf galaxies within the Fornax and Perseus galaxy clusters, derived from *Euclid* ERO, with physically motivated mass models consistent with ΛCDM predictions. For each dwarf galaxy mass model, we generate initial conditions for the associated globular cluster system that reproduce the observed properties. We then evolve these systems forward in time over 10 Gyr to investigate their long-term dynamical evolution.

2.1. GC (candidates) sample

The GC candidate samples are drawn from the two Euclid ERO fields, the Fornax and Perseus clusters, presented by Saifollahi et al. (2025b) and Saifollahi et al. (2025a), respectively. These samples include GC candidates associated with dwarf galaxies in the Fornax cluster (at about 20 Mpc) in the Perseus cluster (at about 72 Mpc). The structural and photometric properties of the dwarf galaxies, including their stellar masses and effective radii, are taken from Saifollahi et al. (2025b) and Venhola et al. (2018) for the Fornax cluster, and Cuillandre et al. (2025b) and Marleau et al. (2025) for the Perseus cluster.

Before investigating the dynamical evolution of *Euclid* globular clusters within their host dwarf galaxies, we apply a set of selection criteria to retain the most robust cluster candidates. The initial ERO sample consists of 47 and 6653 globular clusters, distributed across 16 and 826 dwarf galaxies in the Fornax and Perseus clusters, respectively, with magnitudes in the range $-11.2 < M_{I_E} < -7$ (see Table 1). We retain only clusters with $M_{\rm VIS} < -8$. In addition, we exclude objects with projected radii smaller than 0.2 kpc, as these are more likely to be nuclear star clusters. Applying these criteria reduces our sample to approximately 4500 clusters across both environments, which still provides a statistically significant data set (see Table 1). The globular cluster masses are estimated using:

$$M_{\rm GC} = 1.8 \times 10^{-0.4\,(M_{I_E}+0.5-4.82)}. \tag{1}$$

This equation is given an average $M/L_V = 1.8$ for old metal-poor single stellar populations (Bruzual & Charlot 2003), an average offset of -0.5 between V-band and I_E-band for such stellar population (Saifollahi et al. 2025b in the appendix), and the V-band absolute magnitude of the Sun (Willmer 2018). This results in cluster masses in the range 1.5×10^5 to $3.1 \times 10^6\,M_\odot$ for the selected sample. Finally, the uncertainties on the distances from the galactic centre are small, of the order of a few parsecs. In practice, they are generally smaller than the pixel size, which corresponds to ∼ 10, pc at the distance of Fornax.

2.2. Euclid dwarf galaxies

Each globular cluster is associated with a host dwarf galaxy, which we modelled as a spherical potential following a NFW profile (Navarro et al. 1997b), as predicted by CDM, and characterized by its halo mass M_h and scale radius r_s. We estimate the total dark matter halo mass from the observed stellar mass $M_\star$ by adopting the stellar-to-halo mass relation derived from abundance matching (Behroozi et al. 2010). The dwarf galaxies considered in our sample span stellar masses in the range $4.9 < \log(M_\star/M_\odot) < 9.6$ and dark matter halo masses in the range $9.3 < \log(M_h/M_\odot) < 11.36$. Given the inferred halo mass, the scale radius r_s is determined using results from cosmological N-body simulations (Dutton & Macciò 2014), implemented via the `COLOSSUS` package (Diemer 2018). In models including baryons, the stellar component is represented by a Hernquist profile, parameterised by the observed stellar mass and effective radius.

2.3. Dynamical friction implementation

To compute the dynamics of our GCs over 10 Gyr, it is essential to include dynamical friction in our modelling. This process plays a key role in the deceleration and orbital energy loss of globular clusters within dwarf galaxies. The dynamical friction (DF) force scales with the square of the GC mass and with the local density of the host galaxy, implying that DF is more efficient for massive clusters orbiting in dense environments. The characteristic timescale over which the apocentre of a cluster is significantly reduced by DF can be approximated as

$$t_{\rm fric} \sim \left(\frac{M_{\rm dw}(r)}{M_{\rm GC}}\right) t_{\rm dyn}, \tag{2}$$

where $M_{\rm dw}(r)$ is the mass of the host dwarf galaxy enclosed within the cluster radius r, and $t_{\rm dyn}$ is the dynamical (orbital) timescale (Binney & Tremaine 2008; Bovy 2026). In dwarf galaxies, the enclosed mass in the central regions can be comparable to the mass of a GC, making dynamical friction particularly efficient and capable of driving significant orbital decay on timescales comparable to the Hubble time.

Our implementation of dynamical friction follows Petts et al. (2015), who introduced a semi-analytic model based on the Chandrasekhar (1943) formalism, incorporating radially varying minimum and maximum impact parameters. This approach has been shown to provide excellent agreement with N-body simulations for NFW dark matter distributions, without requiring any parameter fine-tuning. Although the original Chandrasekhar (1943) formalism assumes an infinite and homogeneous background, our implementation partially relaxes this limitation by accounting for the finite size of globular clusters through the inclusion of their half-mass radius, $r_{\rm hm}$, in the Coulomb logarithm. More generally, the validity of this approach can be understood from the fact that dynamical friction in realistic systems arises from resonant interactions, which, when treated as a continuum, recover Chandrasekhar's expression (Tremaine & Weinberg 1984; Weinberg 1986). The formulation of Petts et al. (2015) has been extensively validated against N-body simulations, successfully reproducing the inspiral of globular clusters in spherical halos without parameter tuning. We therefore apply this prescription locally along the orbit, noting that its validity is expected to hold in approximately spherical systems. Extensions to strongly non-spherical environments, such as discs or triaxial galaxies, remain uncertain. Dynamical friction is computed assuming a constant GC mass, as given by Equation (1), and a fixed

Table 1. Globular cluster timing problem in Fornax and Perseus galaxy clusters

	$M_{\rm VIS}$	$N_{\rm GC}$	$N_{\rm dw}$	$N_{\rm dw+NSC}$	$N^{TB}_{\rm GC}$	$N^{TB}_{\rm dw}$	$N^{TB}_{\rm dw+NSC}$	$f^{TB}_{\rm GC}$	$f^{TB}_{\rm dw}$	$f^{TB}_{\rm dw+NSC}$	$\tilde{f}^{TB}_{\rm GC}$	$\tilde{f}^{TB}_{\rm dw}$	$\tilde{f}^{TB}_{\rm dw+NSC}$
Fornax	-	47	16	4									
	-8	39	12	4	9	7	2	0.23	**0.58**	0.16	0.22	**0.56**	0.16
	-9	16	9	2	7	6	2	0.44	**0.67**	0.22	0.41	**0.64**	0.2
Perseus	-	6553	826	226									
	-8	4487	749	181	398	288	76	0.1	**0.38**	0.1	0.08	**0.35**	0.09
	-9	988	406	46	154	135	14	0.15	**0.33**	0.03	0.15	**0.32**	0.03

Notes: From left to right, the columns report the limiting magnitude threshold adopted for the GC sample, the number of GCs, the number of dwarf galaxies, and the number of dwarfs hosting a NSC in our sample. These three quantities are then repeated for the subset of objects exhibiting a timing problem. We further report two types of fractions: the standard fraction f and a weighted fraction $\tilde{f}$, computed for the number of GCs, the number of dwarf galaxies, and the number of dwarfs hosting an NSC that exhibit a timing problem. A dwarf galaxy is identified as hosting an NSC if it contains at least one GC with an observed projected radius < 0.2 kpc, which we classify as an NSC. A GC is considered to exhibit a timing problem if its infalling time is shorter than 10 Gyr, while a dwarf galaxy is considered to have a timing problem if it hosts at least one such GC.

size of 0.01 kpc. This choice corresponds to a conservative upper limit for GC sizes, consistent with the largest systems observed in the MW. Adopting smaller, more typical sizes (e.g., 1–3 pc) would increase the efficiency of dynamical friction and further reduce the infall times. Moreover, direct measurements of the projected sizes of *Euclid* globular clusters will require complementary ground-based observations. Our modelling also relies on the following assumptions for GCs. We assume that the clusters are initialised at positions corresponding to their present-day projected distances, and that they are on circular orbits ($e = 0$) at these radii. GC orbits are evolved for 10 Gyr within a static NFW potential. The integrations are performed using the fast C-based integrator `dop853_c`, implemented in the publicly available code `galpy` (Bovy 2015). In terms of computational performance, evolving $\sim$ 4500 globular clusters over 10 Gyr requires approximately 0.04 CPU hours.

3. Extending Fornax timing problem to local Universe dwarfs

3.1. Fornax-like dwarfs in local Universe

Before revisiting the timing problem, we first aim to clarify how common dwarf galaxies such as Fornax are in the local Universe. To this end, we select Fornax analogues by imposing a stellar mass in the range $2–8 \times 10^7\, M_\odot$, consistent with the observed stellar mass of the Fornax dwarf galaxy. Within this sample, the fraction of analogues strongly depends on the environment. Approximately 42% and 24% of dwarf galaxies in the Fornax and Perseus galaxy clusters in the initial dwarf galaxy samples satisfy these criteria. Among these systems, a subpopulation hosts an NSC, with 16% in the Fornax cluster and 6% in the Perseus cluster. Regarding GCs, Fornax analogues typically host between 1 and 6 GCs. When considering galaxies comparable to the Fornax dSph in GC-richness ($N_{\rm GC} \geq 5$), such systems represent about 16% of the sample, while in Perseus this fraction is 1%.

3.2. GC timing problem in local Universe

To identify which GCs exhibit a timing problem, we consider those whose the apocentre falls below 0.2 kpc after 10 Gyr of orbital integrations. This threshold corresponds to the GC-NSC boundary adopted to clean our sample. This criterion therefore allows us to determine whether a GC has reached the central region of its host galaxy and would have potentially contributed to the formation of a NSC. We recall that we revisit here the classical timing problem, which posits that GCs with ages $\gtrsim$ 10 Gyr are not expected to remain at large radii, but rather to have migrated to the galactic centre due to dynamical friction from field stars and the dark matter halo, where they would have formed an NSC. Based on our GC-NSC boundary, we estimate that 24% (33%) of dwarfs in the Perseus (Fornax) cluster host an NSC (see Table 1). This implies that the majority of dwarfs in these clusters share properties similar to the Fornax dwarf galaxy, namely the presence of GCs within $\sim$ kpc scales (see Figure 1) and the absence of an NSC.

Figure 1 shows the orbits of the 39 GCs associated with dwarfs in the Fornax cluster, centred on their present-day galactocentric distance R, with backward and forward integrations performed both with and without the baryonic component in the galactic potential. A GC is considered to exhibit a timing problem if its infall time is shorter than 10 Gyr, while a dwarf galaxy is considered to have a timing problem if it hosts at least one such GC. We find that 100% (11%) of the Fornax timing problem GCs sink within 6 (2) Gyr. In comparison, for Perseus, 63% (23%) of the timing problem GCs sink within 6 (2) Gyr. As expected, the inclusion of baryons in the galactic potential accelerates orbital decay, as higher central densities enhance dynamical friction. These infall times are short compared to the expected ages of GCs ($>$ 10 Gyr). Overall, we find that 23% of GCs in Fornax exhibit a timing problem, affecting 58% of dwarf galaxies in the cluster. In Perseus, 10% of GCs exhibit a timing problem, corresponding to 38% of dwarf galaxies. Once again, these results suggest that the environment plays a significant role in regulating the fraction of GCs affected by the timing problem. In summary, while the total number of GCs exhibiting a timing problem represents a small fraction of the population, particularly in Perseus, where the statistics are robust, a significant fraction of dwarf galaxies is nevertheless affected. We also note that adopting a stricter magnitude threshold ($M_{\rm VIS} < -9$) does not significantly alter our results (variations of 13–16%), and the timing problem remains (see Table 1). To ensure the robustness of our results, we compute contamination corrected fractions by assigning each *Euclid* GC candidate a probability of being a background contaminant, quantified by p_b. Each candidate is then weighted by its probability of being a genuine GC associated with the host galaxy, defined as $w = 1 - p_b$. All re-

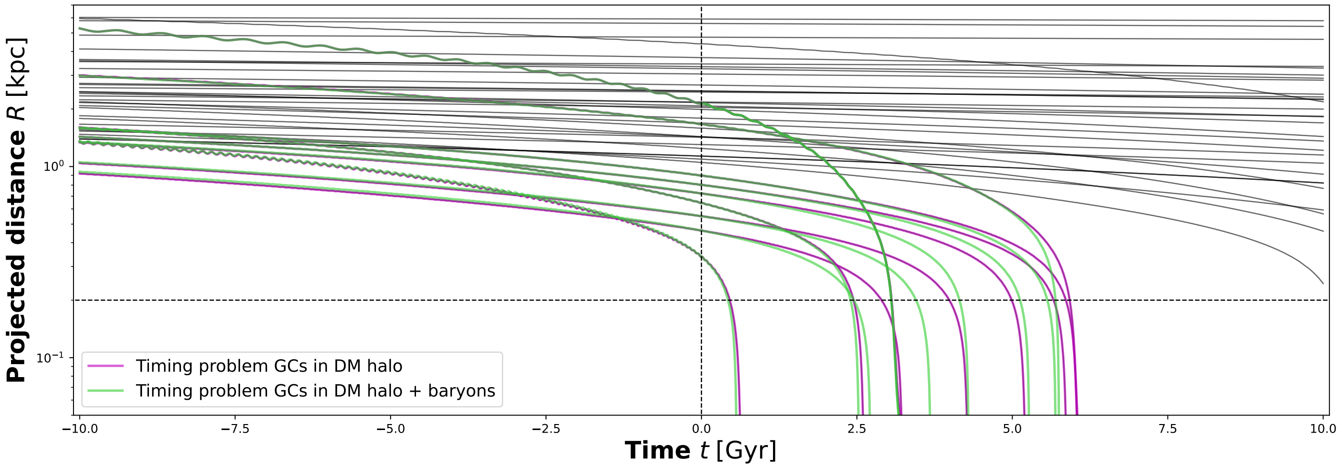

Fig. 1. Orbital evolution of GCs in the Fornax galaxy cluster, assuming their present-day projected distance as the initial position on circular orbits ($e = 0$), present-day GC masses, and a static dwarf galaxy potential derived from the observed stellar mass and calibrated using cosmological CDM simulations. We consider here only GCs with magnitudes brighter than −8. Negative time values correspond to past orbits, while positive values indicate future evolution. The horizontal black dashed line marks the GC-NSC boundary at 0.2 kpc, as defined in this work. Coloured curves highlight GCs exhibiting a timing problem, i.e. those that reach apocentre below 0.2 kpc within 10 Gyr. We find that 23% of GCs in the Fornax cluster exhibit a timing problem, corresponding to 58% of dwarf galaxies hosting at least one such cluster. The inclusion of baryons in the galactic potential accelerates orbital decay.

ported fractions are computed using these weights, thereby estimating the effective contribution of genuine GCs rather than raw candidate counts. For example, two candidates with probabilities of 0.6 and 0.4 correspond to an effective contribution of one genuine GC. Accounting for these weights only marginally affects our results (see Table 1).

Overall, our results reveal that the timing problem is also present in the local Universe. Based on GCs in two independent galaxy clusters, we find that 56% and 35% of dwarf galaxies in the Fornax and Perseus clusters, respectively, exhibit a timing problem. Furthermore, a key result is that the majority of dwarfs exhibiting a timing problem do not host an NSC, with fractions as high as 84% and 91% in Fornax and Perseus, respectively. This significantly reinforces the timing problem, as no cluster-origin object is observed at the galaxy centre, indicating that these GCs have not undergone the expected orbital decay.

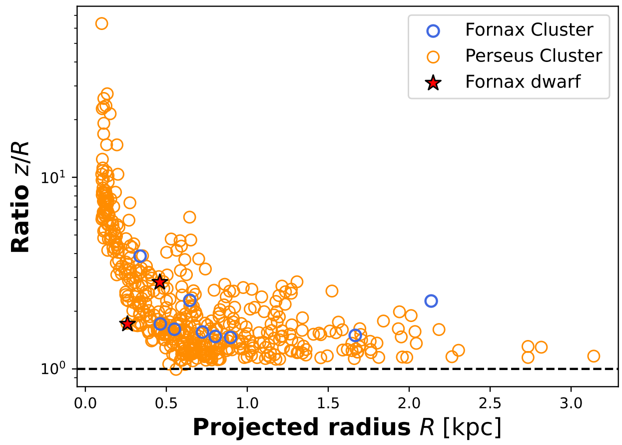

Fig. 2. Required line-of-sight distance z to resolve the timing problem as a function of projected galactocentric radius R. The ratio z/R represents the minimum additional distance along the line of sight needed for each GC to avoid reaching the central region (< 0.2 kpc) within 10 Gyr. Blue and orange circles correspond to GCs in the Fornax and Perseus clusters, respectively, while red stars indicate the GCs of the Fornax dwarf galaxy. The horizontal dashed line marks $z/R = 1$. All GCs require $z \gtrsim R$, with 29% of GCs requiring even more extreme configurations ($z \gtrsim 2R$), highlighting that projection effects alone are unlikely to resolve the timing problem.

3.3. Obvious solutions

As our results suggest the presence of a timing problem in dwarf galaxies in the local Universe, we investigate its robustness against the assumptions underlying the classical Fornax timing problem. In particular, we adopt the following assumptions:

- GCs are located at their projected galactocentric distance,
- GCs are initially on circular orbits,
- the dark matter halo mass is inferred from the stellar-to-halo mass relation of Behroozi et al. (2010).

It is therefore natural to question whether relaxing or refining these assumptions could alleviate or even resolve the timing problem.

3.3.1. Impact of line-of-sight distance uncertainties

A first caveat of our modelling lies in the assumption that GCs start their orbital decay from their projected (2D) galactocentric distance, R. To account for projection effects, it has previously been proposed to introduce an artificial line-of-sight distance of $z = R/\sqrt{3}$, which increases the true galactocentric distance to $\sim 1.15\,R$. In contrast, we estimate here the minimum line-of-sight distance required for each GC to avoid reaching the central region within 10 Gyr, i.e. such that its apocentre remains above 0.2 kpc. Figure 2 clearly shows that all GCs would need to have $z \gtrsim R$ at present in order to alleviate the timing problem in local

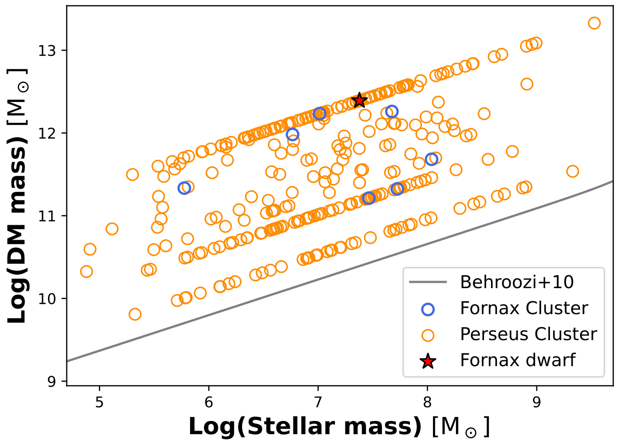

Fig. 3. DM halo mass required to prevent the timing problem as a function of stellar mass. The grey line shows the stellar-to-halo mass relation from Behroozi et al. (2010). Blue and orange circles correspond to dwarf galaxies in the Fornax and Perseus clusters, respectively, while the red star indicates the Fornax dwarf galaxy. Each point represents the minimum halo mass required to keep the apocentre of timing problem GCs above the GC-NSC boundary. A significant fraction of systems requires halo masses well above CDM expectations: 62% of timing problem dwarfs require haloes at least 10 times more massive, 37% require 50 times more massive, and 15% require 100 times more massive haloes

dwarf galaxies. Such a requirement appears highly implausible, as it would imply line-of-sight distances systematically comparable to or larger than the observed projected radii across a wide range of dwarfs and cluster environments. Moreover, we find that 29% of GCs exhibiting a timing problem would require extreme configurations with $z \gtrsim 2R$ (see Figure 2). For comparison, the two timing problem GCs in the Fornax dwarf galaxy would require line-of-sight distances of approximately 2 to 3 times their projected radius. We therefore conclude that uncertainties in the 3D distances alone cannot resolve the timing problem.

3.3.2. Impact of orbital eccentricity

In our modelling, we initially assume circular orbits ($e = 0$) for the GC orbital integrations. This assumption is, however, not fully realistic, as globular clusters are expected to follow eccentric orbits. For instance, GCs in the Milky Way exhibit a mean eccentricity of $e \sim 0.52$ based on *Gaia* data (Gaia Collaboration et al. 2018b). To assess the impact of orbital eccentricity, we re-evaluate the timing problem by considering highly eccentric orbits ($e = 0.9$), representing an extreme case. Figure A.1 shows the orbital evolution of the 39 GCs associated with dwarf galaxies in the Fornax cluster, centred on their present-day galactocentric distance R, with forward integrations performed in a dark matter-only potential describing the host dwarfs. As expected, highly eccentric orbits lead to longer infall times, as the higher initial velocities delay the efficiency of dynamical friction, thereby slowing down orbital decay (see Figures 2 and A.1). Overall, we recover similar fractions of GCs and dwarf galaxies affected by the timing problem in both the Fornax and Perseus galaxy clusters.

3.3.3. Impact of dark matter halo mass uncertainties

A final solution we investigate relies on invoking possible uncertainties in the dark matter halo masses of dwarf galaxies relative to the predictions of the CDM paradigm. Instead of assuming a fixed stellar-to-halo mass relation, we determine the minimum dark matter halo mass required for each dwarf galaxy to prevent the timing problem for its problematic GCs. Specifically, we compute the minimum halo mass such that the apocentre of each GC remains above the GC-NSC boundary at 0.2 kpc.

Figure 3 shows that 62% of timing problem GCs in TB dwarfs would require dark matter haloes at least 10 times more massive than those predicted by CDM. Furthermore, 37% (15%) of cases would require haloes 50 (100) times more massive. Therefore, resolving the timing problem in this framework would require unrealistically massive haloes that are not expected within CDM. We also consider the specific case of the Fornax dwarf galaxy, for which preventing the infall of its two problematic GCs would require a halo mass comparable to that of the Milky Way (see Figure 3).

We conclude that, taken individually, these solutions are insufficient to resolve the timing problem. It is, however, worth exploring whether a combination of these effects could mitigate orbital decay over a Hubble time. Assuming that GCs start at a distance of $1.15\,R$ (i.e. $z = R/\sqrt{3}$) and follow eccentric orbits with $e = 0.52$, we reduce the number of GCs exhibiting a timing problem by approximately a factor of two (194 GCs). Nevertheless, we still find that 59% of timing problem GCs in TB dwarfs require haloes at least 10 times more massive than CDM predictions, while 33% (13%) require haloes 50 (100) times more massive. These constraints are very similar to those obtained under our fiducial assumptions, again pointing toward unrealistic halo masses.

Overall, our results show that, while it is in principle possible to fine-tune the initial conditions to mitigate or even eliminate a fraction of timing problem cases, a robust core of systems remains difficult to reconcile with current theoretical expectations. This suggests that the timing problem cannot be fully resolved by adjusting initial conditions alone, but instead points toward a more fundamental tension in our understanding of globular cluster dynamics within their host gravitational potentials.

4. Discrepancy between high-redshift and local universe GC distance distributions

In order to provide new insights into the timing problem, historically investigated through the forward evolution of GC orbits, we instead adopt a complementary approach by integrating their trajectories backward in time within realistic dwarf galaxy potentials extracted from the hydrodynamical cosmological simulation TNG50 (Nelson et al. 2019b,a; Pillepich et al. 2019). This allows us to better constrain the spatial distribution of *Euclid* GCs at high redshift. As illustrated in Figure 1, backward orbital integrations effectively reverse the role of dynamical friction: instead of acting as an energy loss, it behaves as an energy gain. As a consequence, GCs migrate outward from their present-day positions, reaching galactocentric distances of ∼ 1–5 kpc at lookback times of ∼ 10 Gyr. This motivates us to investigate the impact of dynamical friction on the spatial distribution of GCs at $z \sim 3$.

We consider the most massive galaxy cluster in the TNG50 simulation, which has a virial mass of $1.8 \times 10^{14}\,M_\odot$. Within this halo, we select dwarf galaxies located inside the virial radius (1198.91 kpc) and with stellar masses in the range 10^{6}–$10^{9.5}\,M_\odot$,

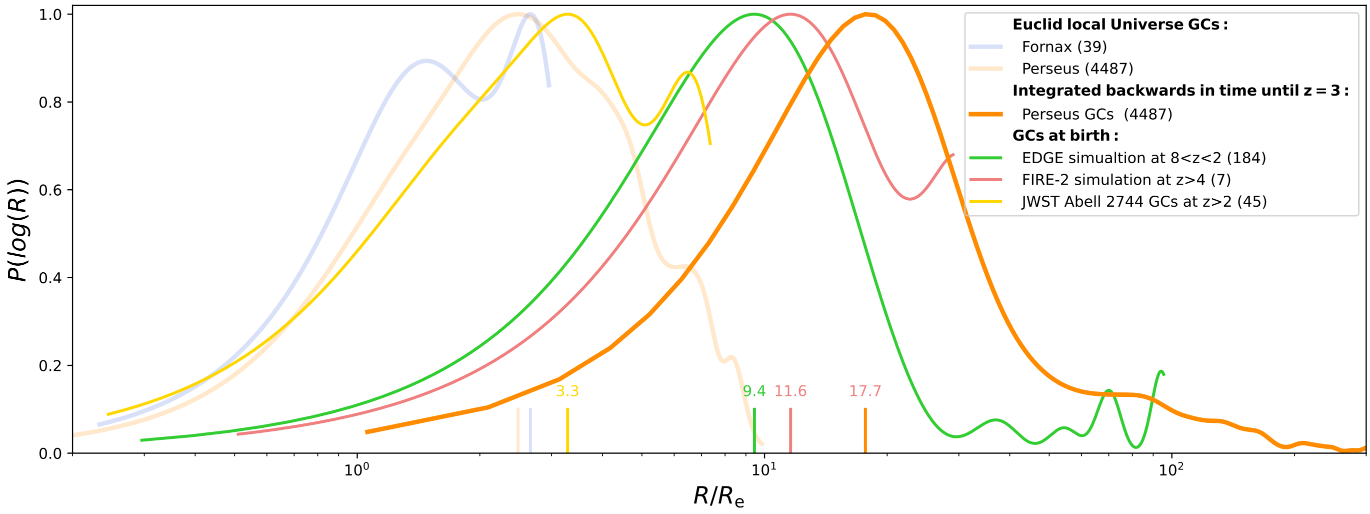

Fig. 4. Probability density of GC projected distance divided by the effective radius R_e for a comparison between observed and simulated data. Vertical lines indicate the median radius of each distribution. There is a significant tension between the backward-integrated positions of *Euclid* Perseus GCs and the expected birth locations inferred from simulations, a discrepancy that is further exacerbated when considering JWST observations. **Pierre: Y axis title should be modified**

consistent with the mass range of *Euclid* dwarf galaxies. Among the 848 dwarfs identified in TNG50, we successfully match 660 systems to the 749 galaxies observed in the Perseus by *Euclid*, requiring a stellar mass agreement better than 5%. The matching is performed on a one-to-one basis by minimizing stellar mass differences. We then construct time-evolving gravitational potentials that account for the evolution of dwarf galaxies within the TNG cluster environment, in particular through mass accretion and stripping processes. Specifically, Pillepich et al. (2019) provide stellar masses and half-mass radii at multiple redshifts for all galaxies identified in the most massive cluster. Each dwarf galaxy is modelled using a Hernquist (1990) profile for the stellar component and a Navarro–Frenk–White (NFW) profile (Navarro et al. 1997b) for the DM halo, with parameters calibrated from TNG50 outputs. As in previous sections, we assume circular orbits initialised at the projected galactocentric distances observed by *Euclid* in order to reconstruct their past evolution. This assumption corresponds to minimally radial trajectories and therefore yields a lower bound on orbital excursions. Consequently, the reconstructed radii should be regarded as conservative estimates, as more eccentric orbits—expected to be more representative of realistic trajectories—would lead to significantly larger spatial displacements.

Finally, each GC is integrated backward in time down to $z = 3$ within its matched TNG50 dwarf galaxy potential, including the effects of dynamical friction while assuming constant GC mass and size. This assumption likely minimizes the impact of dynamical friction, as higher masses and more compact sizes would enhance its efficiency. This methodology is applied exclusively to the Perseus sample, as the Fornax system does not provide sufficient statistics for a robust analysis.

4.1. *Euclid* Perseus GCs locations at $z = 3$

Figure 4 shows the probability density distribution of GC projected distance, $P(\log R)$, divived by the effective radius R_e, for the *Euclid* Perseus sample reconstructed at $z = 3$, in comparison with high-resolution simulations and JWST observations. The effective radius is estimated assuming $R_e = 0.015\, r_{200}$, where

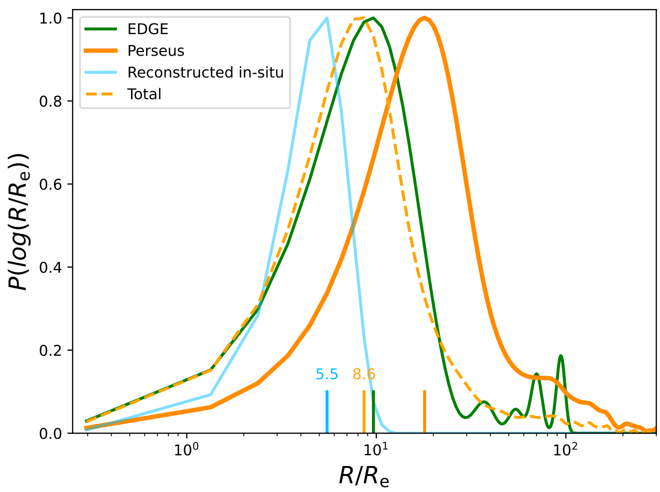

Fig. 5. Probability density of GC projected distance divided by the effective radius R_e. **Pierre: Add $z = 3$ for Perseus**

r_{200} denotes the virial radius of the host dwarf galaxy (Kravtsov 2013). Local Fornax and Perseus GC system display relatively concentrated distributions around $R/R_e \sim 1$–3 (see high transparency blue and orange curves in Figure 4). In contrast, backward integration of the Perseus GC system to $z = 3$ leads to a significant shift of the distribution toward larger radii, with a peak at $R/R_e \sim 18$. This suggests that GCs currently observed in the inner regions were initially located at much larger galactocentric distances. For comparison, we include results from the EDGE Taylor et al. (2025) and FIRE Sameie et al. (2023) high-resolution simulations, which contain 184 and 7 GCs, respectively. The green and red curves, derived from EDGE ($8 < z < 2$) and FIRE-2 ($z > 4$), trace the spatial distribution of GCs at formation, with peaks around $R/R_e \sim 9$ and ~ 12, showing clear tension with the reconstructed high-redshift distribution.

Recent observations with *JWST*/NIRCam have provided data for 537 strongly magnified galaxies in the redshift range $0.7 < z < 10$ in the galaxy clusters fields Abell 2744 and AbellS 1063

Claeyssens et al. 2025, 2026 identified and analysed 2370 compact stellar clumps in these fields using gravitational lensing with sizes ranging from 1 to 500 pc. Clump sizes and fluxes were derived by fitting PSF-convolved elliptical 2D Gaussian profiles (following the method of Claeyssens et al. 2025). Intrinsic effective radii ($R_{\rm eff}$) are PSF-deconvolved and corrected for lensing magnification, with upper limits assigned to unresolved clumps. Stellar masses were derived via SED fitting with Bagpipes (Bayesian Analysis of Galaxies for Physical Inference and Parameter EStimation, Carnall et al. (2019)), using BPASS v2.2.1 templates and exponential-declining star formation histories (τ = 1 Myr, approximating a single burst), with free parameters including age, formed stellar mass, metallicity, dust attenuation, and ionisation parameter. Host galaxy properties were also obtained via SED fitting with Bagpipes, using the non-parametric continuity SFH model of Leja et al. (2019) with 10–14 age bins (depending on redshift) to constrain both recent (<100 Myr) and older (>300 Myr) star formation episodes. Stellar masses are corrected from magnification to obtain the intrinsic stellar mass of each clump and galaxy. To measure galactocentric distances of the clumps within their host galaxy, the intrinsic (source-plane) morphology of each galaxy is first reconstructed by directly inverting the lensing equation pixel by pixel. This reconstruction is performed without PSF deconvolution, however, the sharp NIRCam PSF does not significantly affect the global source-plane morphology, then this reconstruction is reliable enough to identify the central clump, defined as the clump closest to the light barycenter. The same source-plane projection is then used to project the observed clumps position to their intrinsic position and then compute the distance of each clump from their host galaxy center, yielding its galactocentric distance. It should be noted, however, that identifying a well-defined center is more robust for evolved, bulge-hosting galaxies (mostly z < 2.5) than for young, strongly irregular high-redshift galaxies. We applied a series of selection criteria to this catalogue to retain only robust and physically meaningful sources. First, we selected objects with projected galactocentric distances in the range $0.2 < R < 10$ kpc, excluding both NSCs and distant outliers. We then restricted the sample to high-redshift systems with $z > 2$. In addition, we imposed a cut on the effective radius, requiring $R_{\rm eff} \leq 40$ pc, thereby removing overly extended structures unlikely to correspond to compact star-forming clumps or proto-GC candidates. We further selected only systems with masses above $6\times10^6\,M_\odot$ to ensure their survival down to $z = 0$. The resulting JWST sample with 45 objects at $z > 2$ provides an even stronger discrepancy, as the peak of the distribution ($R/R_e \sim 3$) lies very close to the present-day *Euclid* distribution (see yellow curve in Figure 4).

Overall, these results reveal a significant tension between the backward-integrated positions of *Euclid* Perseus GCs and the birth locations inferred from both cosmological simulations and JWST observations. We therefore emphasize that the primary challenge is not merely to resolve the classical GC timing problem itself, which may naturally disappear once the full orbital evolution of GCs is properly accounted for, but rather to establish a consistent connection between the high-redshift Universe and the GC populations observed in the local Universe. In this context, the timing problem should instead be regarded as only the tip of the iceberg, namely the visible manifestation of a broader and more fundamental issue related to the long-term orbital evolution, migration, and survival of GCs across cosmic time. Motivated by this discrepancy presented in Figure 4, we explore scenarios that could reconcile these contrasting spatial distributions at high redshift. We emphasize that our modelling likely underestimates the impact of dynamical friction due to our assumptions of circular orbits and constant cluster mass and size, making this tension potentially even more severe. In the following, we investigate the realism and implications of two scenarios within the ΛCDM framework. We note, however, that their validity may be limited in alternative DM models such as warm DM or self-interacting DM and fuzzy DM, where differences in hierarchical structure formation, dark matter distribution, and dynamical friction could significantly alter the predicted GC spatial distributions.

4.2. Scenario 1: A domination by ex-situ GCs

A first scenario that naturally emerges is the possibility of a strong observational bias in the *Euclid* data. This interpretation relies on the fact that the observed GC population only represents the surviving GCs at $z = 0$. Indeed, a significant fraction of the initial GC population, particularly the in-situ component, is expected to have either been disrupted by tidal effects or to have sunk toward the centre of their host galaxies through dynamical friction, eventually contributing to the formation of a NSC. We therefore investigate whether the absence of this primordial in-situ population could reconcile the discrepancy between the backward-integrated *Euclid* distributions and the expected GC birth distributions.

However, a first difficulty immediately emerges. Simulations predict that most GCs form at normalised radii around $R/R_{\rm e} \sim 12$, whereas our backward integrations suggest typical birth radii almost twice as large (see Figure 4). The discrepancy becomes even more severe when considering JWST observations, which instead indicate a peak around $R/R_{\rm e} \sim 3$. This implies that neither simulations nor observations support the formation of GCs at the large radii inferred from our backward integrations. Consequently, the present-day GC population would necessarily have to be largely dominated by ex-situ GCs. Since clusters cannot realistically form at such large radii, the only remaining possibility is that they formed closer to the centres of other dwarf galaxies and were later accreted through mergers. Such a scenario is nevertheless rather extreme, as it implicitly assumes that the majority of the original in-situ population either disappeared or migrated toward the centres of dwarf galaxies, leading to the formation of NSCs.

In order to quantify how extreme this scenario is, we estimated the missing in-situ population required to reproduce the radial peak predicted by the EDGE simulation using the backward-integrated *Euclid* Perseus sample shown in Figure 4. We chose to calibrate this reconstructed population on the EDGE simulation because it provides the best statistics among the available data sets, with a sample of 184 GCs. The goal is to determine the number of missing in-situ GCs that must be added to the Perseus sample at $z = 3$ in order to recover the radial distribution predicted by EDGE, in particular the location of the peak. To achieve this, we introduce a synthetic in-situ population drawn from a Gaussian distribution centred on the EDGE peak, with a fixed dispersion of 0.2 kpc. This choice effectively restricts GC formation to within $\sim$ 1 kpc from the galaxy centre. The number of added GCs is then iteratively adjusted until the peak positions agree within a tolerance of 0.01 kpc. Figure 5 shows the probability density distribution of projected GC distances for both the reconstructed in-situ population and the total population (reconstructed in-situ + backward-integrated Perseus sample at $z = 3$). This procedure reveals that at least $\sim$ 9000 in-situ GCs are required to realign the distributions, corresponding to nearly twice the number of observed *Euclid* Perseus clus-

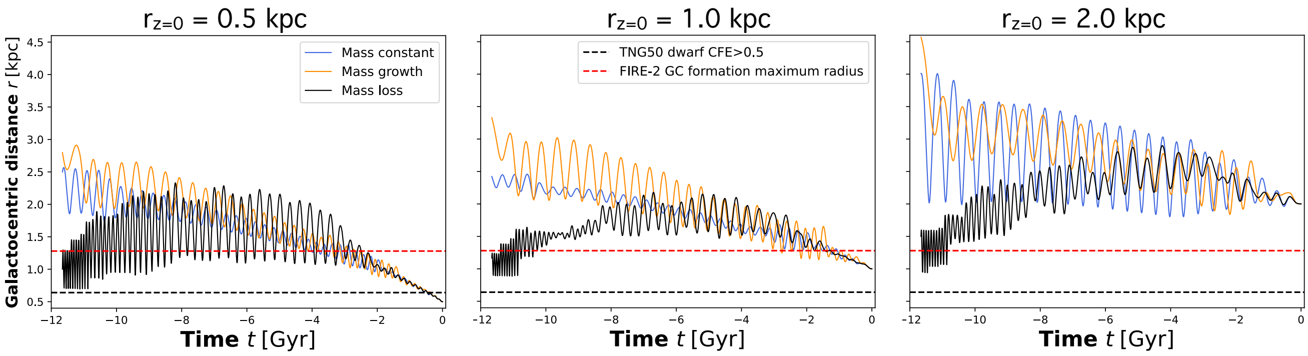

Fig. 6. Evolution of GC galactocentric distances integrated backward in time under different host halo mass evolution scenarios. The three panels show the orbital evolution of GCs initialised at present-day galactocentric distances of $r_{z=0}$ = 0.5, 1.0, and 2.0 kpc, respectively. The blue, orange, and black curves correspond to constant halo mass, halo mass growth, and halo mass loss scenarios. **Pierre: remove red and black dashed lines**

ters (4487). The reconstructed in-situ population peaks around 5.5 R_e, in good agreement with both simulations and JWST observations. Our results therefore imply that an extremely large fraction of the primordial GC population, of the order of ∼ 2/3, must have disappeared by $z = 0$.

To further emphasize how extreme this requirement is, we computed the orbital evolution of GCs initialised at $z = 3$ in all dwarf galaxies identified in the TNG50 cluster, adopting an initial radius of $r = 5.5\,R_e$, corresponding to the peak of the reconstructed in-situ distribution. The orbits of $10^5\,M_\odot$ GCs were then integrated forward to $z = 0$ within the evolving dwarf potentials. We find that, in 74% of the dwarfs, all clusters starting within 5.5 R_e end up below 0.2 kpc at $z = 0$, corresponding to our adopted GC–NSC transition radius. This result confirms that such an initial distribution naturally leads to the inspiral of a large fraction of the reconstructed population of ∼ 9000 GCs. On average, this corresponds to roughly ∼ 10 clusters per dwarf at $z = 3$ having a high probability of sinking toward the centre within a Hubble time and contributing to NSC formation. Observationally, however, only 27% of Perseus dwarfs host an NSC. This discrepancy therefore further strengthens the conclusion that such a scenario is unlikely.

In addition, the full assembly history of the 660 dwarf galaxies identified in the TNG50 cluster can be reconstructed. Whenever a merger occurred, we identified the most massive satellite galaxy involved in the interaction, corresponding to the "next progenitor" in the TNG50 merger trees. We find that 67% of the dwarfs experienced no mergers with galaxies more massive than $10^6\,M_\odot$ in stellar mass. This result directly contradicts a scenario in which the GC population is predominantly ex-situ. Furthermore, the 23% of dwarfs that did experience mergers could collectively contribute only ∼ 583 GCs, compared to the ∼ 4000 GCs observed by *Euclid*. The total number of globular clusters is estimated assuming a linear proportionality between the GC population and the dark matter mass of each dwarf galaxy, $N_{GC} \propto M_{dm}$. We adopt an optimistic high-redshift scaling relation of $M_{GC}/M_h = 10^{-3}$ following Choksi & Gnedin (2019), while local observational constraints typically favour lower values in the range 10^{-4}–10^{-5}. Although the specific assembly history of the TNG50 cluster may differ from that of Perseus, it nevertheless appears highly implausible that mergers alone could increase the GC population by an order of magnitude. Overall, these results strongly indicate that the contribution of the in-situ population is essential and that present-day GC systems are most likely composed of a mixture of in-situ and ex-situ clusters. Taken together, all these elements suggest that a scenario dominated by ex-situ GCs is unlikely within the standard CDM framework.

4.3. Scenario 2: Missing friction-counteracting mechanisms

Figures 4 and 5 reveal two important implications. First, preserving the in-situ GC population over cosmic time appears to require mechanisms capable of either reducing dynamical friction itself or counteracting the resulting orbital decay. Second, such mechanisms are absent from our current modelling. Their omission is therefore likely responsible for part of the tension between the backward-integrated *Euclid* distributions and the expected GC birth distributions inferred from simulations and JWST observations. In particular, the results obtained in Scenario 1 showed that, in most dwarf galaxies, clusters born within ∼ 5.5 R_e are expected to inevitably sink toward the centre of the host galaxy, reaching radii below 0.2 kpc between $z = 3$ and $z = 0$ in our TNG50 dwarf sample. This leaves little room for the survival of the JWST GC population, whose distribution peaks around ∼ 3.3 R_e. One would therefore expect an even larger fraction of clusters to experience orbital decay and eventually contribute to the formation of a central nuclear star cluster. This further strengthens the idea that additional physical processes must act to slow down, stall, or counterbalance GC inspiral over cosmic time in order to preserve the mixed in-situ and ex-situ populations that are clearly observed today in the MW.

Another striking feature is that the peaks of the *Euclid* GC distribution at $z = 0$ and the JWST distribution at $z > 2$ remain located at similar normalised radii, around ∼ 2–4 R_e. However, galaxies are expected to grow cosmologically, with effective radii evolving on average as $R_e \propto (1 + z)^{-1.1}$ (van der Wel et al. 2014; Shibuya et al. 2015). If GC systems were unaffected by the host galaxy evolution, one would therefore expect the ratio R/R_e to decrease with cosmic time. The fact that the peak position remains approximately constant instead suggests that GC systems evolve roughly homologously with their host galaxies, with clusters migrating outward proportionally to the galaxy size growth. This points toward the absence of strong differential radial migration, implying that dynamical friction cannot dominate the long-term evolution of the bulk of massive GCs. This argument becomes even stronger in dwarf galaxies, where the majority of systems experience no significant mergers after $z = 3$ (67% in the most massive TNG50 galaxy cluster). This suggests that GCs must stay relatively close to their birth locations in order to preserve the observed normalised radial distributions over cosmic time.

In the following, we discuss several candidate mechanisms that could either directly reduce the efficiency of dynamical friction or counteract the orbital decay induced by it, and assess their potential to alleviate the tension highlighted by our results.

4.3.1. Intrinsic reduction of dynamical friction

Several mechanisms have been proposed that can intrinsically reduce the efficiency of dynamical friction by modifying either the underlying DM distribution or the global gravitational response of dwarf galaxies. Among the most commonly discussed candidates are:

- DM mass loss
- DM cores
- dynamical buoyancy within such cores.

In the standard hierarchical framework, galaxies are expected to grow through mergers and accretion. However, this picture can be significantly altered in dense environments such as galaxy clusters, where strong tidal interactions may efficiently strip mass from satellite dwarf galaxies. This is particularly relevant for the *Euclid* dwarf sample studied here, which resides in a cluster environment. As a consequence, three broad evolutionary scenarios can be distinguished for dwarf halos: constant mass, halo growth, and halo mass loss. Figure 6 illustrates the orbital evolution of GCs under these different assumptions. In the constant-mass case, clusters remain confined within a relatively narrow radial range and mainly experience the gradual inward migration expected from dynamical friction. In contrast, halo mass growth progressively shifts clusters toward larger galactocentric distances at high redshift when integrating backward in time, due to the shrinking of the host potential. Conversely, halo mass loss can induce an orbital expansion of GCs that initially formed in the inner regions of their host galaxies. As the dwarf galaxy progressively loses DM through tidal stripping, the shallowing of the gravitational potential causes cluster orbits to expand toward larger galactocentric distances. However, once the halo mass evolution stabilizes, dynamical friction becomes efficient again and gradually drives clusters back toward the inner regions of the galaxy. Overall, these results demonstrate that the cosmological evolution of the host halo potential can significantly modify the inferred birth locations of present-day GCs. Although halo mass loss may therefore contribute to orbital expansion and partially counteract GC inspiral, our results indicate that this mechanism alone is insufficient to explain the observed distributions. Indeed, the cosmological evolution of dwarf galaxy masses is already included in our orbital integrations, yet the tension between backward-integrated *Euclid* clusters and the expected GC birth distributions remains.

Another possibility is the presence of central DM cores. In the standard CDM framework, DM halos are expected to develop cuspy density profiles that diverge toward the centre. However, numerous observational studies have suggested that some galaxies instead host central cores with nearly constant-density inner profiles (McGaugh et al. 2001b; Oh et al. 2015b; **?**; Santos-Santos et al. 2020b).Such cores can naturally reduce the efficiency of dynamical friction by lowering the central DM density. In addition, DM cores are expected to induce a phenomenon known as core stalling, in which the orbital decay of a perturber strongly slows down or even ceases once it approaches the core radius (Read et al. 2006b; Inoue 2011; Cole et al. 2012b; Dutta Chowdhury et al. 2019). This mechanism has been extensively discussed as a possible solution to the long-standing timing problem of the Fornax dwarf galaxy. In particular, several studies have argued that cores of order ~ 1 kpc are required to prevent the inspiral of the Fornax GC population (Goerdt et al. 2006b; Sánchez-Salcedo et al. 2006b; Leung et al. 2020b). The physical origin of such cores in the CDM framework nevertheless remains highly debated. A large number of hydrodynamical simulations have linked core formation to bursty stellar feedback processes (Pontzen & Governato 2012; Di Cintio et al. 2014; Tollet et al. 2016). In particular, repeated supernova-driven gas outflows may transfer energy to the DM component and flatten the inner density profile. It has also been suggested that sustained late-time star formation is necessary to maintain these cores over cosmic time (Read et al. 2019; Muni et al. 2025). However, recent simulations have highlighted a far more complex picture. The EDGE simulations presented by Muni et al. (2025) show that DM core formation critically depends on the timing of star formation relative to cosmic reionization. Similarly, the FIRE-3 simulations including AGN feedback by Koudmani et al. (2025) indicate that the interaction between AGN activity and cosmic rays may paradoxically favour the reformation of cuspy profiles by suppressing late-time star formation. Analytical models further suggest that AGN energetics could be particularly efficient in the dwarf galaxy regime compared to stellar feedback alone (Silk 2017; Dashyan et al. 2018). Yet the impact of AGN feedback in dwarf galaxies is itself expected to be highly stochastic and strongly dependent on uncertain black hole seeding prescriptions, with some dwarfs potentially hosting no central black hole at all. Conversely, other numerical studies find little or no correlation between stellar feedback and core formation. For instance, the LYRA simulations presented by Sureda et al. (2026) report no clear connection between star formation activity and the emergence of DM cores, in agreement with the results of Bose et al. (2019) and Benítez-Llambay et al. (2019), who instead find the persistence of cuspy profiles or even halo contraction.

Overall, the strong discrepancies between current hydrodynamical simulations, combined with the sensitivity of the results to numerical implementations and feedback prescriptions, indicate that DM core formation within the ΛCDM framework remains fundamentally uncertain. In particular, there is currently no robust prediction for the characteristic size of DM cores within the ΛCDM framework. Besides stellar and AGN feedback, galaxy mergers have also been suggested as a possible mechanism for flattening the inner DM density profile. However, the resulting cores appear to remain relatively modest in size. Using merger simulations of cuspy CDM halos ($\gamma > 1$) in dwarfs, Goerdt et al. (2010) found that merger-induced cores typically do not exceed ~ 300 pc, substantially smaller than the $\gtrsim 1$–1.5 kpc cores generally required to efficiently suppress dynamical friction in systems such as the Fornax dwarf galaxy.

An even more intriguing phenomenon associated with DM cores is dynamical buoyancy. First identified by Cole et al. (2012b), this effect occurs when perturbers initially located within a DM core begin to migrate outward instead of inward. In this regime, dynamical friction not only becomes inefficient, but may even reverse sign. At first sight, dynamical buoyancy appears to provide an extremely promising mechanism for preventing GC inspiral and preserving extended in-situ GC populations. However, recent work by Dattathri et al. (2025) suggests that buoyancy only occurs for a restricted class of dynamically unstable core profiles, occupying a much narrower parameter space than that of large stable cores. Moreover, these authors demonstrate that this dynamical friction behaviour is not uniquely tied to a specific density slope, further complicating the interpretation. Therefore, although dynamical buoyancy constitutes one of the most efficient known mechanisms for counteracting orbital decay, its viability ultimately depends on the existence of large DM cores whose formation and stability remain highly uncertain within the standard CDM framework.

4.3.2. Friction-counteracting mechanisms

Besides processes that intrinsically reduce dynamical friction through modifications of the dark matter distribution, several mechanisms may instead counteract GC orbital decay through dynamical perturbations, stochastic heating, or environmental effects. Among the most relevant candidates are:

- dwarf galaxy mergers
- DM subhalo interactions
- the non-spherical DM halos.

In our model, the time evolution of the dark matter halo mass and scale radius already accounts for the global evolution of the host potential, including the averaged effect of hierarchical assembly. However, individual merger events are not explicitly modelled. As a consequence, transient perturbations associated with mergers are absent from our orbital integrations, despite their potentially important impact on GC dynamics. Depending on the geometry and mass ratio of the interaction, mergers can either contract or expand GC orbits through violent gravitational perturbations (Naab et al. 2009). Such merger-driven orbital expansion could therefore contribute to maintaining clusters at large galactocentric radii and help alleviate the timing problem identified in our backward integrations.

Although major mergers between dwarf galaxies become relatively rare after $z \sim 3$, minor interactions may still play an important role in shaping GC orbital evolution over cosmic time. In particular, repeated gravitational perturbations induced by mergers may inject orbital energy into GCs and partially counterbalance the inward migration expected from dynamical friction. The CDM paradigm predicts the existence of a very large population of dark matter substructures within galactic halos (Springel et al. 2008; Diemand et al. 2008). As dark matter halos grow hierarchically through the continuous accretion of smaller halos, these subhalos interact gravitationally with the various components of galaxies before eventually being disrupted. It has been estimated that dwarf halos of mass $\sim 10^9$–$10^{10}\,M_\odot$ may accrete between ~ 10 and ~ 14 subhalos with mass ratios $10 < M_{\rm host}/M_{\rm sub} < 100$ throughout their assembly history (Neistein & Dekel 2008). These repeated interactions can effectively be interpreted as a sequence of minor mergers capable of continuously perturbing the host galaxy. Recent studies have shown that subhalo interactions can dynamically heat stellar systems through stochastic energy injection, producing a gradual and self-similar expansion of the stellar distribution (Vitral et al. 2026). In particular, subhalo crossings have been proposed as a mechanism capable of displacing central black holes from galaxy centres through repeated dynamical perturbations (Boldrini et al. 2020b). By analogy, the same mechanism may also dynamically heat GC systems and counteract orbital decay. Applied to our framework, such stochastic heating processes may naturally contribute to maintaining GCs at larger radii than predicted by standard dynamical friction models.

Another mechanism that could naturally reduce the efficiency of dynamical friction is the non-sphericity of the host dark matter halo (Jeeson-Daniel et al. 2011). Both simulations and observations have long established that dark matter halos are not simply spherical systems (Allgood et al. 2006; Hayashi et al. 2007; Butsky et al. 2016; Suto et al. 2016; Prada et al. 2019; Despali et al. 2013; Kasun & Evrard 2005; Orkney et al. 2023). Instead, they generally exhibit triaxial shapes characterized by three distinct principal axes of different lengths. This triaxiality naturally emerges from the complex anisotropic gravitational interactions governing halo formation and hierarchical assembly. In such non-spherical systems, the orbital evolution of satellites and globular clusters can differ significantly from the classical spherical case. In particular, Peñarrubia et al. (2002) showed that dynamical friction in flattened dark matter halos becomes strongly anisotropic, with the orbital decay timescale depending sensitively on the inclination and orientation of the orbit. In particular, satellites on polar or highly inclined orbits can survive significantly longer than in the classical spherical case. Peñarrubia et al. (2002) further found that the range of satellite survival times in flattened halos can become up to $\sim 100\%$ larger than in spherical halos, highlighting the major impact of halo geometry on orbital evolution. This effect is particularly relevant for our study because all orbital integrations presented in this work assume spherical dark matter potentials. If real dwarf halos are flattened or triaxial, the efficiency of dynamical friction could therefore be substantially overestimated in our model. In that case, non-spherical potentials may naturally help prevent the rapid inward migration of GCs toward the galaxy centre and contribute to preserving extended in-situ populations.

Overall, all the friction-counteracting mechanisms discussed above are intrinsically stochastic and are expected to vary significantly from one dwarf galaxy to another depending on their individual assembly histories and environments. It is therefore unlikely that a single mechanism alone is responsible for suppressing GC orbital decay. Instead, the long-term survival of GCs at large galactocentric radii probably results from the combined action of several of these processes operating simultaneously over cosmic time.

5. Conclusion

Acknowledgements. PB and TS acknowledges funding from the CNES postdoctoral fellowship programme. The Euclid Consortium acknowledges the European Space Agency and a number of agencies and institutes that have supported the development of *Euclid*, in particular the Agenzia Spaziale Italiana, the Austrian Forschungsförderungsgesellschaft funded through BMK, the Belgian Science Policy, the Canadian Euclid Consortium, the Deutsches Zentrum für Luft- und Raumfahrt, the DTU Space and the Niels Bohr Institute in Denmark, the French Centre National d'Etudes Spatiales, the Fundação para a Ciência e a Tecnologia, the Hungarian Academy of Sciences, the Ministerio de Ciencia, Innovación y Universidades, the National Aeronautics and Space Administration, the National Astronomical Observatory of Japan, the Netherlandse Onderzoekschool Voor Astronomie, the Norwegian Space Agency, the Research Council of Finland, the Romanian Space Agency, the State Secretariat for Education, Research, and Innovation (SERI) at the Swiss Space Office (SSO), and the United Kingdom Space Agency. A complete and detailed list is available on the *Euclid* web site (`www.euclid-ec.org`). This work has made use of the Early Release Observations (ERO) data from the *Euclid* mission of the European Space Agency (ESA), 2024, `https://doi.org/10.57780/esa-qmocze3`. This research has made use of the SIMBAD database (Wenger et al. 2000), operated at CDS, Strasbourg, France, the VizieR catalogue access tool (Ochsenbein et al. 2000), CDS, Strasbourg, France (DOI : 10.26093/cds/vizier), and the Aladin sky atlas (Bonnarel et al. 2000; Boch & Fernique 2014) developed at CDS, Strasbourg Observatory, France and SAOImageDS9 (Joye & Mandel 2003). This work has been done using the following software, packages and python libraries: `Topcat` (Taylor 2005); `Numpy` (van der Walt et al. 2011), `Scipy` (Virtanen et al. 2020), `Astropy` (Astropy Collaboration et al. 2018), `Scikit-learn` (Pedregosa et al. 2011).

References

Adams, J. J., Simon, J. D., Fabricius, M. H., et al. 2014, ApJ, 789, 63
Allgood, B., Flores, R. A., Primack, J. R., et al. 2006, MNRAS, 367, 1781
Amorisco, N. C., Agnello, A., & Evans, N. W. 2013, MNRAS, 429, L89

Arca-Sedda, M. & Capuzzo-Dolcetta, R. 2016, MNRAS, 461, 4335
Astropy Collaboration, Price-Whelan, A. M., Sipőcz, B. M., et al. 2018, AJ, 156, 123
Battaglia, G., Helmi, A., & Breddels, M. 2013, New A Rev., 57, 52
Battaglia, G., Sollima, A., & Nipoti, C. 2015, MNRAS, 454, 2401
Battaglia, G., Tolstoy, E., Helmi, A., et al. 2006, A&A, 459, 423
Behroozi, P. S., Conroy, C., & Wechsler, R. H. 2010, ApJ, 717, 379
Benítez-Llambay, A., Frenk, C. S., Ludlow, A. D., & Navarro, J. F. 2019, MNRAS, 488, 2387
Binney, J. & Tremaine, S. 2008, Galactic Dynamics: Second Edition (Princeton, NJ: Princeton University Press)
Boch, T. & Fernique, P. 2014, in Astronomical Society of the Pacific Conference Series, Vol. 485, Astronomical Data Analysis Software and Systems XXIII, ed. N. Manset & P. Forshay, 277
Boldrini, P. 2021, Galaxies, 10, 5
Boldrini, P., Mohayaee, R., & Silk, J. 2019, MNRAS, 485, 2546
Boldrini, P., Mohayaee, R., & Silk, J. 2020a, MNRAS, 492, 3169
Boldrini, P., Mohayaee, R., & Silk, J. 2020b, MNRAS, 495, L12
Bonnarel, F., Fernique, P., Bienaymé, O., et al. 2000, A&AS, 143, 33
Borukhovetskaya, A., Errani, R., Navarro, J. F., Fattahi, A., & Santos-Santos, I. 2022, MNRAS, 509, 5330
Bose, S., Frenk, C. S., Jenkins, A., et al. 2019, MNRAS, 486, 4790
Bovy, J. 2015, ApJS, 216, 29
Bovy, J. 2026, Dynamics and Astrophysics of Galaxies (Princeton, NJ: Princeton University Press; in press)
Brook, C. B. 2015, MNRAS, 454, 1719
Bruzual, G. & Charlot, S. 2003, MNRAS, 344, 1000
Bullock, J. S. & Boylan-Kolchin, M. 2017, ARA&A, 55, 343
Burkert, A. 2015, ApJ, 808, 158
Butsky, I., Macciò, A. V., Dutton, A. A., et al. 2016, MNRAS, 462, 663
Carnall, A. C., Leja, J., Johnson, B. D., et al. 2019, ApJ, 873, 44
Chandrasekhar, S. 1943, ApJ, 97, 255
Choksi, N. & Gnedin, O. Y. 2019, MNRAS, 488, 5409
Claeyssens, A., Adamo, A., Kokorev, V., et al. 2026, arXiv e-prints, arXiv:2601.16281
Claeyssens, A., Adamo, A., Messa, M., et al. 2025, MNRAS, 537, 2535
Cole, D. R., Dehnen, W., Read, J. I., & Wilkinson, M. I. 2012a, MNRAS, 426, 601
Cole, D. R., Dehnen, W., Read, J. I., & Wilkinson, M. I. 2012b, MNRAS, 426, 601
Cowsik, R., Wagoner, K., Berti, E., & Sircar, A. 2009, ApJ, 699, 1389
Cuillandre, J.-C., Bertin, E., Bolzonella, M., et al. 2025a, A&A, 697, A6
Cuillandre, J.-C., Bolzonella, M., Boselli, A., et al. 2025b, A&A, 697, A11
Dashyan, G., Silk, J., Mamon, G. A., Dubois, Y., & Hartwig, T. 2018, MNRAS, 473, 5698
Dattathri, S., van den Bosch, F. C., Banik, U., et al. 2025, arXiv e-prints, arXiv:2511.11804
de Boer, T. J. L. & Fraser, M. 2016, A&A, 590, A35
Despali, G., Tormen, G., & Sheth, R. K. 2013, MNRAS, 431, 1143
Di Cintio, A., Brook, C. B., Macciò, A. V., et al. 2014, MNRAS, 437, 415
Diemand, J., Kuhlen, M., Madau, P., et al. 2008, Nature, 454, 735
Diemer, B. 2018, ApJS, 239, 35
Dinescu, D. I., Keeney, B. A., Majewski, S. R., & Girard, T. M. 2004, AJ, 128, 687
Dutta Chowdhury, D., van den Bosch, F. C., & van Dokkum, P. 2019, ApJ, 877, 133
Dutton, A. A. & Macciò, A. V. 2014, MNRAS, 441, 3359
Errani, R., Peñarrubia, J., & Walker, M. G. 2018, MNRAS, 481, 5073
Fattahi, A., Navarro, J. F., Frenk, C. S., et al. 2018, MNRAS, 476, 3816
Flores, R. A. & Primack, J. R. 1994, ApJ, 427, L1
Forbes, D. A., Read, J. I., Gieles, M., & Collins, M. L. M. 2018, MNRAS, 481, 5592
Gaia Collaboration, Helmi, A., van Leeuwen, F., et al. 2018a, A&A, 616, A12
Gaia Collaboration, Helmi, A., van Leeuwen, F., et al. 2018b, A&A, 616, A12
Garrison-Kimmel, S., Hopkins, P. F., Wetzel, A., et al. 2019, MNRAS, 487, 1380
Genina, A., Read, J. I., Fattahi, A., & Frenk, C. S. 2022, MNRAS, 510, 2186
Goerdt, T., Moore, B., Read, J. I., & Stadel, J. 2010, ApJ, 725, 1707
Goerdt, T., Moore, B., Read, J. I., Stadel, J., & Zemp, M. 2006a, MNRAS, 368, 1073
Goerdt, T., Moore, B., Read, J. I., Stadel, J., & Zemp, M. 2006b, MNRAS, 368, 1073
Hayashi, E., Navarro, J. F., & Springel, V. 2007, MNRAS, 377, 50
Hernandez, X. & Gilmore, G. 1998, MNRAS, 297, 517
Hernquist, L. 1990, ApJ, 356, 359
Inoue, S. 2009, MNRAS, 397, 709
Inoue, S. 2011, MNRAS, 416, 1181
Jeeson-Daniel, A., Dalla Vecchia, C., Haas, M. R., & Schaye, J. 2011, MNRAS, 415, L69
Joye, W. A. & Mandel, E. 2003, in Astronomical Society of the Pacific Conference Series, Vol. 295, Astronomical Data Analysis Software and Systems XII, ed. H. E. Payne, R. I. Jedrzejewski, & R. N. Hook, 489
Kaplinghat, M., Tulin, S., & Yu, H.-B. 2016, Phys. Rev. Lett., 116, 041302
Kasun, S. F. & Evrard, A. E. 2005, ApJ, 629, 781
Kaur, K. & Sridhar, S. 2018, ApJ, 868, 134
Koudmani, S., Rennehan, D., Somerville, R. S., et al. 2025, MNRAS, 540, 1928
Kravtsov, A. V. 2013, ApJ, 764, L31
Larsen, S. S., Strader, J., & Brodie, J. P. 2012, A&A, 544, L14
Leja, J., Carnall, A. C., Johnson, B. D., Conroy, C., & Speagle, J. S. 2019, ApJ, 876, 3
Leung, G. Y. C., Leaman, R., van de Ven, G., & Battaglia, G. 2020a, MNRAS, 493, 320
Leung, G. Y. C., Leaman, R., van de Ven, G., & Battaglia, G. 2020b, MNRAS, 493, 320
Lux, H., Read, J. I., & Lake, G. 2010, MNRAS, 406, 2312
Mackey, A. D. & Gilmore, G. F. 2003, MNRAS, 340, 175
Marleau, F., Cuillandre, J.-C., Cantiello, M., et al. 2025, A&A, 697, A12
Mateo, M. L. 1998, ARA&A, 36, 435
McGaugh, S. S., Rubin, V. C., & de Blok, W. J. G. 2001a, AJ, 122, 2381
McGaugh, S. S., Rubin, V. C., & de Blok, W. J. G. 2001b, AJ, 122, 2381
Meadows, N., Navarro, J. F., Santos-Santos, I., Benítez-Llambay, A., & Frenk, C. 2020, MNRAS, 491, 3336
Moore, B. 1994, Nature, 370, 629
Muni, C., Pontzen, A., Read, J. I., et al. 2025, MNRAS, 536, 314
Munshi, F., Brooks, A. M., Applebaum, E., et al. 2021, ApJ, 923, 35
Naab, T., Johansson, P. H., & Ostriker, J. P. 2009, ApJ, 699, L178
Navarro, J. F., Frenk, C. S., & White, S. D. M. 1996, ApJ, 462, 563
Navarro, J. F., Frenk, C. S., & White, S. D. M. 1997a, ApJ, 490, 493
Navarro, J. F., Frenk, C. S., & White, S. D. M. 1997b, ApJ, 490, 493
Neistein, E. & Dekel, A. 2008, MNRAS, 388, 1792
Nelson, D., Pillepich, A., Springel, V., et al. 2019a, MNRAS, 490, 3234
Nelson, D., Springel, V., Pillepich, A., et al. 2019b, Computational Astrophysics and Cosmology, 6, 2
Ochsenbein, F., Bauer, P., & Marcout, J. 2000, A&AS, 143, 23
Oh, K. S., Lin, D. N. C., & Richer, H. B. 2000, ApJ, 531, 727
Oh, S.-H., Brook, C., Governato, F., et al. 2011, AJ, 142, 24
Oh, S.-H., Hunter, D. A., Brinks, E., et al. 2015a, AJ, 149, 180
Oh, S.-H., Hunter, D. A., Brinks, E., et al. 2015b, AJ, 149, 180
Oman, K. A., Navarro, J. F., Fattahi, A., et al. 2015, MNRAS, 452, 3650
Orkney, M. D. A., Taylor, E., Read, J. I., et al. 2023, MNRAS, 525, 3516
Peñarrubia, J., Kroupa, P., & Boily, C. M. 2002, MNRAS, 333, 779
Peñarrubia, J., Navarro, J. F., & McConnachie, A. W. 2008, ApJ, 673, 226
Pedregosa, F., Varoquaux, G., Gramfort, A., et al. 2011, Journal of Machine Learning Research, 12, 2825
Petts, J. A., Gualandris, A., & Read, J. I. 2015, MNRAS, 454, 3778
Piatek, S., Pryor, C., Olszewski, E. W., et al. 2002, AJ, 124, 3198
Pietrzyński, G., Górski, M., Gieren, W., et al. 2009, AJ, 138, 459
Pillepich, A., Nelson, D., Springel, V., et al. 2019, MNRAS, 490, 3196
Pontzen, A. & Governato, F. 2012, MNRAS, 421, 3464
Prada, J., Forero-Romero, J. E., Grand, R. J. J., Pakmor, R., & Springel, V. 2019, MNRAS, 490, 4877
Read, J. I. & Erkal, D. 2019, MNRAS, 487, 5799
Read, J. I., Goerdt, T., Moore, B., et al. 2006a, MNRAS, 373, 1451
Read, J. I., Goerdt, T., Moore, B., et al. 2006b, MNRAS, 373, 1451
Read, J. I., Walker, M. G., & Steger, P. 2019, MNRAS, 484, 1401
Saifollahi, T., Lançon, A., Cantiello, M., et al. 2025a, A&A, 703, A184
Saifollahi, T., Voggel, K., Lançon, A., et al. 2025b, A&A, 697, A10
Sameie, O., Boylan-Kolchin, M., Hopkins, P. F., et al. 2023, MNRAS, 522, 1800
Sánchez-Salcedo, F. J. & Lora, V. 2022, MNRAS, 511, 1860
Sánchez-Salcedo, F. J., Reyes-Iturbide, J., & Hernandez, X. 2006a, MNRAS, 370, 1829
Sánchez-Salcedo, F. J., Reyes-Iturbide, J., & Hernandez, X. 2006b, MNRAS, 370, 1829
Santos-Santos, I. M. E., Navarro, J. F., Robertson, A., et al. 2020a, MNRAS, 495, 58
Santos-Santos, I. M. E., Navarro, J. F., Robertson, A., et al. 2020b, MNRAS, 495, 58
Schive, H.-Y., Chiueh, T., & Broadhurst, T. 2014, Nature Physics, 10, 496
Shao, S., Cautun, M., Frenk, C. S., et al. 2021, MNRAS, 507, 2339
Shibuya, T., Ouchi, M., & Harikane, Y. 2015, ApJS, 219, 15
Silk, J. 2017, ApJ, 839, L13
Springel, V., Wang, J., Vogelsberger, M., et al. 2008, MNRAS, 391, 1685
Strigari, L. E., Bullock, J. S., Kaplinghat, M., et al. 2006, ApJ, 652, 306
Sureda, J., Brown, S. T., Fattahi, A., et al. 2026, MNRAS, 548, stag709
Suto, D., Kitayama, T., Nishimichi, T., Sasaki, S., & Suto, Y. 2016, PASJ, 68, 97
Taylor, E. D., Read, J. I., Orkney, M. D. A., et al. 2025, Nature, 645, 327
Taylor, M. B. 2005, in Astronomical Society of the Pacific Conference Series, Vol. 347, Astronomical Data Analysis Software and Systems XIV, ed. P. Shopbell, M. Britton, & R. Ebert, 29

Tollet, E., Macciò, A. V., Dutton, A. A., et al. 2016, MNRAS, 456, 3542
Tremaine, S. & Weinberg, M. D. 1984, MNRAS, 209, 729
Tremaine, S. D. 1976, ApJ, 203, 345
Tremaine, S. D., Ostriker, J. P., & Spitzer, Jr., L. 1975, ApJ, 196, 407
van der Walt, S., Colbert, S. C., & Varoquaux, G. 2011, Computing in Science and Engineering, 13, 22
van der Wel, A., Franx, M., van Dokkum, P. G., et al. 2014, ApJ, 788, 28
Venhola, A., Peletier, R., Laurikainen, E., et al. 2018, A&A, 620, A165
Virtanen, P., Gommers, R., Oliphant, T. E., et al. 2020, Nature Methods, 17, 261
Vitral, E. & Boldrini, P. 2022, A&A, 667, A112
Vitral, E., Peñarrubia, J., & Walker, M. G. 2026, MNRAS, 546, staf2013
Walker, M. 2013, in Planets, Stars and Stellar Systems. Volume 5: Galactic Structure and Stellar Populations, ed. T. D. Oswalt & G. Gilmore, Vol. 5, 1039
Walker, M. G., Mateo, M., & Olszewski, E. W. 2009, AJ, 137, 3100
Walker, M. G. & Peñarrubia, J. 2011, ApJ, 742, 20
Wang, L., Dutton, A. A., Stinson, G. S., et al. 2015, MNRAS, 454, 83
Wang, M. Y., Koposov, S., Drlica-Wagner, A., et al. 2019, ApJ, 875, L13
Weinberg, M. D. 1986, ApJ, 300, 93
Wenger, M., Ochsenbein, F., Egret, D., et al. 2000, A&AS, 143, 9
Willmer, C. N. A. 2018, ApJS, 236, 47
Wolf, J., Martinez, G. D., Bullock, J. S., et al. 2010, MNRAS, 406, 1220

---

[1] LIRA, Observatoire de Paris, Université PSL, Sorbonne Université, Université Paris Cité, CY Cergy Paris Université, CNRS, 92190 Meudon, France
[2] Université de Strasbourg, CNRS, Observatoire astronomique de Strasbourg, UMR 7550, 67000 Strasbourg, France
[3] Univ Lyon, Univ Lyon1, Ens de Lyon, CNRS, CRAL UMR5574, F-69230, Saint-Genis-Laval, France

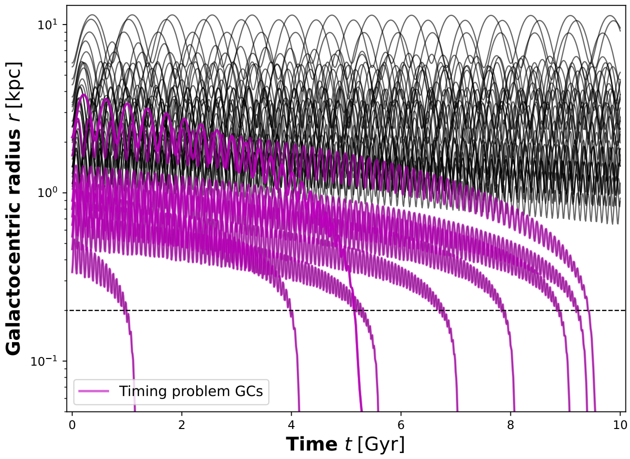

Fig. A.1. Similar to Figure 1 but GCs on eccentric orbits ($e = 0.9$). Highly eccentric orbits lead to longer infall times but we recovered similar fractions of GCs and dwarf galaxies affected by the timing problem in both the Fornax and Perseus galaxy clusters.

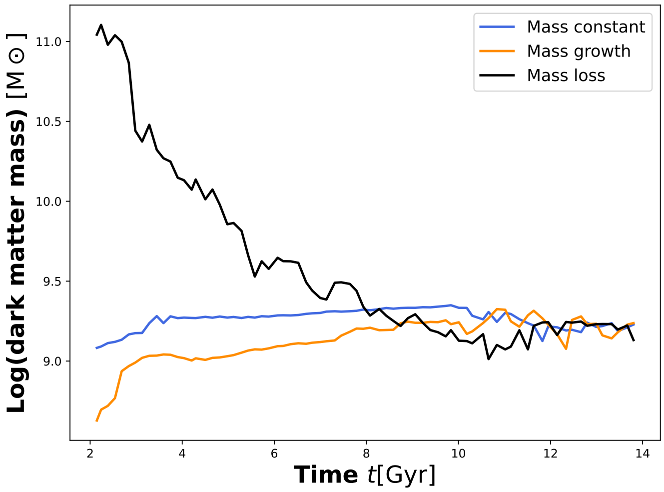

Fig. B.1. Evolution of the dark matter halo mass as a function of cosmic time between $z = 3$ and $z = 0$ for three dwarf galaxies extracted from the TNG50 simulation. We show three representative evolutionary scenarios: a static halo with constant mass (blue), a dwarf halo experiencing gradual mass growth (orange), and a dwarf halo undergoing mass loss (black).

Appendix A: Impact of orbital eccentricity

Appendix B: Different evolution of dwarf dark matter mass from TNG50 simulation